FISEVIER

Contents lists available at ScienceDirect

Materials Today Energy

journal homepage: www.journals.elsevier.com/materials-today-energy/



High-performance all-solid-state lithium batteries enabled by a highly adhesive dry-processable binder

Jiho Cha^a, Young-Jun Lee^a, Dong-Won Kim^{a,b,*}

- ^a Department of Chemical Engineering, Hanyang University, Seoul, 04763, Republic of Korea
- b Department of Battery Engineering, Hanyang University, Seoul, 04763, Republic of Korea

ARTICLE INFO

Keywords:
All-solid-state batteries
Composite cathode
Sulfide electrolyte
Dry processing
Polymer binder

ABSTRACT

All-solid-state lithium batteries (ASSLBs) have emerged as a promising solution to the safety concerns associated with traditional lithium-ion batteries. In sulfide-based ASSLBs, polytetrafluoroethylene (PTFE) binder is typically used for fabricating sheet-type composite cathodes via a solvent-free dry process. However, PTFE presents limitations in achieving desirable cycling stability and high-rate performance. In this study, we introduce a highly adhesive dry-processable binder, poly(tetrafluoroethylene-co-2,2,4-trifluoro-5-trifluoromethoxy-1,3-dioxole) (P(TFE-TTD)), designed to enhance electrochemical performance of ASSLBs. The all-solid-state lithium cell assembled using $\text{Li}_6\text{PS}_5\text{Cl}$ electrolyte, composite $\text{LiNi}_{0.8}\text{Co}_{0.1}\text{Mn}_{0.1}\text{O}_2$ cathode employing P(TFE-TTD) binder demonstrated an impressive discharge capacity of 183.8 mAh g⁻¹ (2.2 mAh cm⁻²), with superior cycling stability of 87 % retention after 200 cycles at 0.5 C and 25 °C. This improved performance is attributed to enhanced interfacial adhesion between cathode components and reduced electrical resistance. Our findings highlight the potential of P(TFE-TTD) as an effective binder material for preparing high-performance dry-processed composite cathodes in the all-solid-state batteries.

1. Introduction

The excessive reliance on fossil fuels has led to severe environmental challenges and energy crises. To mitigate these issues, the development of sustainable, renewable energy technologies along with efficient energy storage systems is essential [1,2]. Among various storage solutions, lithium-ion batteries (LIBs) have emerged as the dominant technology, owing to their high energy density and long cycle life [3-6]. This is especially true in the electric vehicle (EV) industry, where the demand for high-energy-density LIBs is rapidly increasing. However, the flammable and volatile organic liquid electrolytes used in conventional LIBs raise significant safety concerns [7,8]. To address this, all-solid-state lithium batteries (ASSLBs) have been proposed as a promising alternative [9-12]. By replacing flammable liquid electrolytes with solid-state materials, ASSLBs offer enhanced safety and improved cycle life. Furthermore, solid electrolytes enable the use of lithium metal anodes, which significantly boost energy density [13-17]. Among various solid electrolyte systems, argyrodite-type crystalline materials such as Li₆PS₅X (X = Cl, Br, or I) have demonstrated high ionic conductivities $(>10^{-3} \text{ S cm}^{-1})$ [18,19]. In addition to their excellent ionic transport, their soft nature and mechanical deformability make them favorable for

large-scale fabrication of ASSLBs [19-23]. Composite cathodes in ASSLBs are typically fabricated using either wet or dry processing techniques. The wet process involves dissolving a polymeric binder in a solvent to mix with active materials and conductive carbon, forming a slurry [24,25]. However, sulfide-based solid electrolytes are unstable in polar solvents, leading to the substantial drop in ionic conductivity [26, 27]. This incompatibility limits the choice of polymer binders with strong adhesive properties and often necessitates a high binder content, which increases the electrode's electrical resistance. In contrast, the dry process avoids solvents by using shear force to fibrillate polytetrafluoroethylene (PTFE) binder, which interweaves the cathode components [28-32]. PTFE is well known for its excellent electrochemical stability at high voltages and good chemical compatibility with sulfide-based solid electrolytes. Although fibrous PTFE offers certain benefits, it fails to provide strong interfacial adhesion among cathode components [33]. Furthermore, its insulating nature lowers the overall electrical conductivity of the composite electrode [34,35]. Therefore, the development of adhesive binders with lower electrical resistance is essential for achieving high-performance ASSLBs with enhanced cycle life and high-rate capability.

In this study, we propose a highly adhesive, dry-processable PTFE-

^{*} Corresponding author. Department of Chemical Engineering, Hanyang University, Seoul, 04763, Republic of Korea. *E-mail address:* dongwonkim@hanyang.ac.kr (D.-W. Kim).

based copolymer binder, poly(tetrafluoroethylene-co-2,2,4-trifluoro-5-trifluoromethoxy-1,3-dioxole) (P(TFE-TTD)) for the fabrication of composite cathodes in ASSLBs. The composite cathodes incorporating P (TFE-TTD) binder were systematically investigated in terms of morphology, interfacial adhesion, mechanical integrity, and electrochemical performance. Additionally, theoretical modeling was conducted to further elucidate the enhanced adhesive properties of binder. An all-solid-state cell composed of a Li-In alloy anode, Li₆PS₅Cl electrolyte, and an NCM composite cathode incorporating the P(TFE-TTD) binder achieved a high discharge capacity of 183.8 mAh g⁻¹ and demonstrated good cycling stability during cycling at 0.5 C and 25 °C.

2. Material and methods

2.1. Materials

P(TFE-TTD) ($M_n=1.36\times10^5~g~mol^{-1}$) and PTFE ($M_n=1.2\times10^6~g~mol^{-1}$) binders were purchased from Sigma-Aldrich. The P(TFE-TTD) copolymer consists of 40 mol% tetrafluoroethylene (TFE) and 60 mol% 2,2,4-trifluoro-5-trifluoromethoxy-1,3-dioxole (TTD). Li_6PS_5Cl solid electrolyte ($d_{50}=1.0~\mu m$) was obtained from Jeong Kwan Co., Ltd., and carbon nanofibers purchased from Sigma-Aldrich were used as the conductive agent. $LiNi_{0.8}Co_{0.1}Mn_{0.1}O_2$ (NCM) cathode material ($d_{50}=4.0~\mu m$, Fig. S1) was supplied by L&F Co., Ltd. Prior to use, all solid components including Li_6PS_5Cl , carbon nanofibers, and NCM were vacuum-dried overnight at $100~^\circ C$. The surface of the NCM particles was modified with a boron-containing layer to prevent undesirable interfacial reactions with the Li_6PS_5Cl electrolyte. Lithium and indium foils were obtained from Honjo Metal and Nilaco, respectively.

2.2. Electrode preparation and solid-state cell assembly

The composite NCM cathode was prepared by thoroughly mixing NCM, Li $_6$ PS $_5$ Cl, carbon nanofiber, and binder (70:25:3:2 by weight) using a mortar and pestle for 1 h, as shown in Fig. S2a. The dry-processed composite cathode was then obtained by compressing the resulting flake under a pressure of 430 MPa. The active material in the composite cathode was loaded at around 12.0 mg cm $^{-2}$. Separately, 100 mg of Li $_6$ PS $_5$ Cl solid electrolyte powder was pelletized into a 700 µm-thick pellet under a pressure of 300 MPa. To ensure intimate interfacial contact, the prepared composite cathode was placed on the solid electrolyte pellet and compressed at 430 MPa. Subsequently, a Li-In foil anode comprising lithium and indium (1:2 by molar ratio) was positioned on the opposite side of the solid electrolyte pellet. The all-solid-state cell was assembled by applying a final torque of 75 MPa (Fig. S2b). All fabrication steps were carried out in a high-purity argon-filled glove box (H $_2$ O and O $_2$ levels <0.1 ppm, MBRAUN).

2.3. Electrochemical measurements

AC impedance spectra were recorded in the frequency range of 1 MHz–10 mHz with an applied amplitude of 10 mV. Prior to the main cycling tests, two pre-conditioning cycles were conducted at 0.05 C rate and 25 °C. The cells were then subjected to galvanostatic charge and discharge cycling within a voltage window of 2.4–3.7 V (vs. Li-In) at a current density of 0.5 C (where 1.0 C corresponds to 2.2 mA cm⁻²) and 25 °C. After constant current-charging, a constant-voltage of 3.7 V was applied until the current dropped to 10 % of the initial charging current (0.05 C). The rate capability test involved cycling the cell at various Crates from 0.05 C to 1.0 C. DC-IR was extracted by analyzing the slope of the voltage change versus current, based on previously reported procedures [36,37]. Following pre-conditioning, the cell was charged to 3.1 V and rested for 1 h. For each C-rate (ranging from 0.05C to 1.0 C), the test protocol involved a 10-s charge pulse, a 20-min rest, a 10-s discharge pulse, and another 20-min rest period.

2.4. Characterization

To identify the chemical structure of the polymer binders, FT-IR spectroscopy was performed using a Nicolet iS50 (Thermo Fisher Scientific) over the range of 400–1600 cm $^{-1}$. Scanning electron microscopy (SEM, Verios G4 UC) was utilized to investigate the cross-sectional and surface morphologies of the samples, and energy-dispersive X-ray spectroscopy (EDS, Nova NanoSEM 450) was employed to perform elemental analysis. The cohesive strength of the composite cathodes was evaluated using a surface and interfacial cutting analysis system (SAI-CAS, Daipla Wintes Co., Ltd). The elastic properties of the composite cathodes were further assessed through nanoindentation measurements using a NanoTest NTX system.

3. Results and discussion

The two polymer binders, PTFE and P(TFE-TTD), used in composite cathode preparation, were analyzed for their chemical structure via FT-IR spectroscopy. Fig. S3a and S3b show the chemical structures of PTFE and P(TFE-TTD), respectively. The main functional groups (TFE and TTD units) in both polymers were identified by their FT-IR spectra (Fig. S3c and S3d). Both binders exhibit characteristic absorption bands corresponding to the –CF2–CF2– backbone [38]. In addition to the peaks associated with PTFE, new absorption bands appear at 1066 and 1286 cm⁻¹ in the FT-IR spectrum of P(TFE-TTD), which can be attributed to C–F and C–O stretching vibrations, respectively [39].

Cross-sectional SEM images and their EDS elemental mapping were obtained to examine the morphology of the composite cathodes, as presented in Fig. 1. The distribution of each component within the composite cathode was analyzed using EDS mapping: Ni from the NCM, S from the Li₆PS₅Cl, C from the carbon nanofiber and binder, and F from the polymer binder. The SEM image of the PTFE-based composite cathode reveals fiber-like structures of the polymer binder (Fig. 1a), which is consistent with previous reports [40,41]. In contrast, the composite cathode incorporating P(TFE-TTD) shows a more uniform binder distribution (Fig. 1b) and exhibits point-contact binding, unlike the fiber-like binding characteristic of PTFE.

The SAICAS test was performed to evaluate and compare the cohesive strength of composite cathodes prepared with different binders. Horizontal and vertical forces were recorded during the cutting and peeling modes, respectively (Fig. S4). As shown in Fig. 2a and b, both forces were higher in the electrode prepared with P(TFE-TTD) binder, indicating superior cohesive properties compared to those of PTFE. The elastic recovery behavior of composite cathodes containing PTFE and P (TFE-TTD) binders was investigated through nanoindentation testing. Based on the load-depth curves presented in Fig. 2c, the elastic recovery ratio was obtained by calculating the ratio between the recovered and maximum penetration depth. The elastic recovery ratios of the two composite cathodes with different binders are shown in Fig. 2d. The P (TFE-TTD)-based composite cathode exhibits a higher elastic recovery ratio, suggesting that this binder more effectively accommodates volume changes associated with the intercalation and deintercalation of Li+ ions in the active materials. These results demonstrate that the P(TFE-TTD) binder imparts enhanced cohesive strength and elastic recovery to the composite cathode, making it a more effective binder for maintaining structural integrity during battery operation.

To elucidate the binding properties between the polymer binder and the NCM surface, density functional theory (DFT) calculations were conducted, with computational details provided in the Supporting Information. The TFE unit in PTFE and the TTD unit in P(TFE-TTD) were identified as the primary binding sites with metal atoms (Ni, Co, and Mn) on the NCM(104) surface, as illustrated in Fig. 3a. The DFT results reveal that the TTD group in P(TFE-TTD) exhibits binding energies of -0.322, -0.340, and -0.350 eV at the Ni, Co, and Mn sites, respectively. In contrast, the TFE unit in PTFE shows weaker binding energies of -0.029, -0.149, and -0.086 eV at the same respective sites (Fig. 3b).

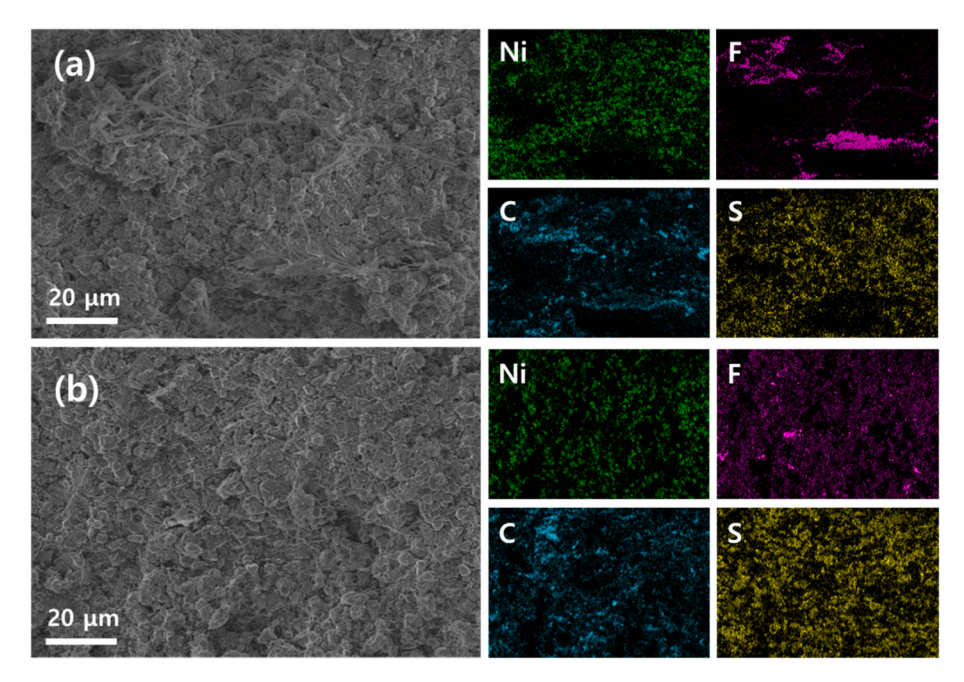


Fig. 1. Cross-sectional SEM images of composite cathodes prepared with (a) PTFE and (b) P(TFE-TTD), and corresponding EDS mapping images (Ni, F, C, and S).

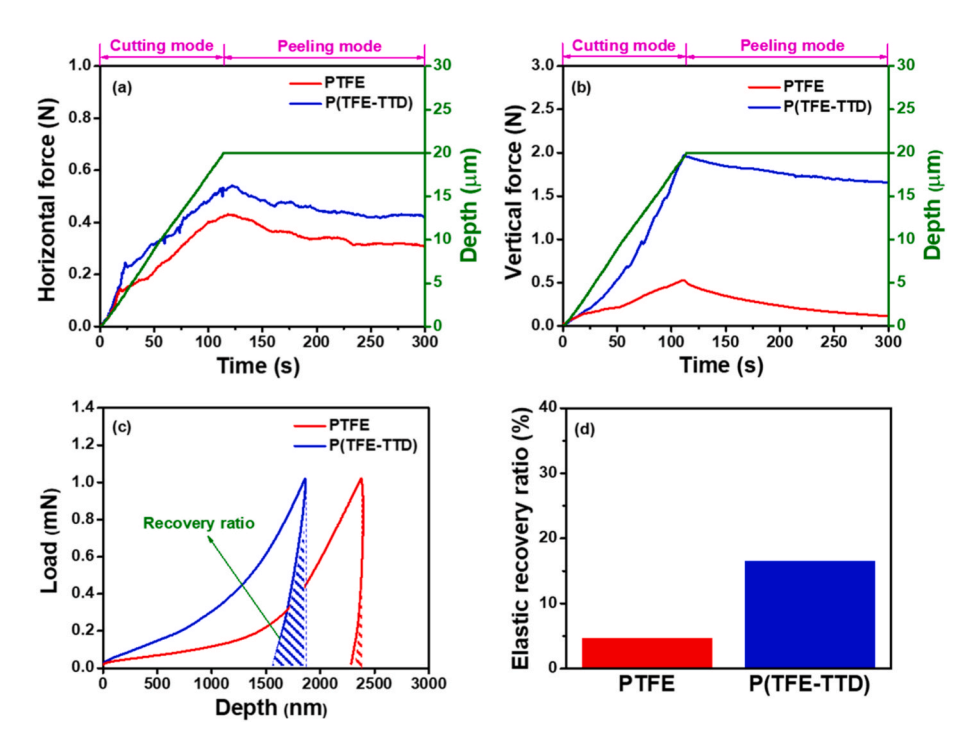


Fig. 2. (a) Horizontal and (b) vertical forces required to cut and peel the composite cathodes employing different binders. (c) Nanoindentation load-depth curves and (d) elastic recovery ratio of composite cathodes with PTFE and P(TFE-TTD) binders.

Additional calculations were performed to investigate the interaction between the monomer units and the NCM(003) and $\rm Li_6PS_5Cl(001)$ surfaces. The binding sites involving Li atoms on these surfaces are identified in Fig. S5. As shown in Fig. S6, the TTD group demonstrates significantly stronger binding energies than the TFE unit on both the NCM(003) and $\rm Li_6PS_5Cl(001)$ surfaces. These findings indicate a stronger affinity of cathode components for TTD over TFE, which accounts for the enhanced adhesive properties of the P(TFE-TTD) binder. NCM particles were coated with 0.5 mol% of lithium boron oxide. To provide a comprehensive understanding of the effect of the boron-containing surface layer, DFT calculations were also conducted to investigate the

interaction between the TTD unit in P(TFE-TTD) and the boron-containing layer on the NCM(003) surface, as the surface modification plays a critical role in determining interfacial behavior. The binding sites on the coating layer are identified in Fig. S7a. As shown in Fig. S7b, the TTD group exhibits significantly stronger binding energy on the boron-coated NCM(003) surface compared to the bare NCM(003) surface. These results suggest that the cohesive strength with the P(TFE-TTD) binder can be enhanced by introducing a surface coating layer on the NCM.

It is essential to investigate whether any undesired interfacial reactions occur between the binder and either ${\rm Li_6PS_5Cl}$ or NCM in the

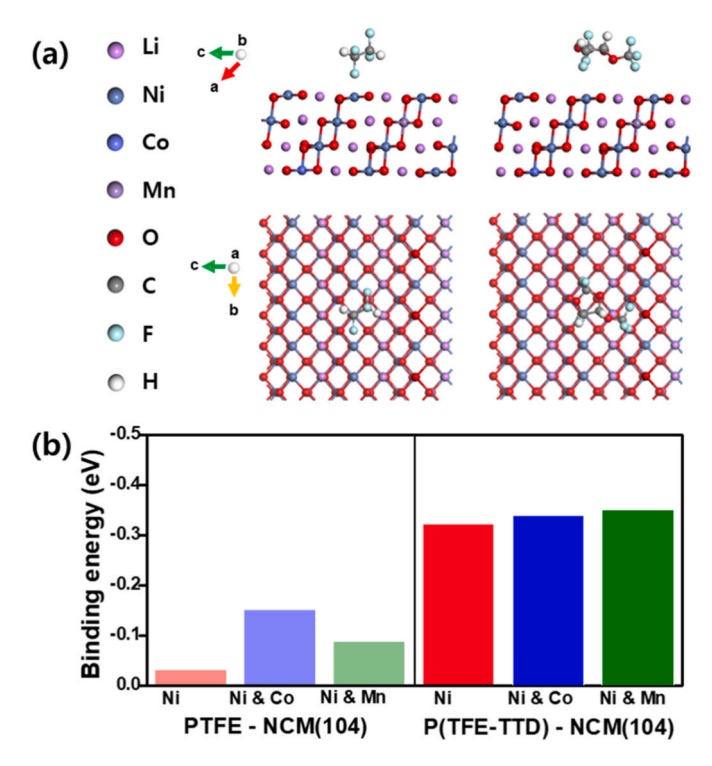


Fig. 3. Theoretical binding energies of binders: (a) The optimized geometric structures of TFE and TFE-TTD monomers on the (104) surface of NCM. (b) Comparison of the theoretical binding energies.

composite cathode. To examine this, we performed XRD analysis of the composite cathode over time (Fig. S8). The results confirm that the composite cathode exhibits the same characteristic diffraction peaks corresponding to crystalline $\text{Li}_6\text{PS}_5\text{Cl}$ and NCM, with no additional peaks or peak shifts observed. These findings indicate that both NCM and $\text{Li}_6\text{PS}_5\text{Cl}$ exhibit good chemical stability with the P(TFE-TTD) binder, without any undesired interfacial reactions in the composite cathode.

In an effort to optimize the amount of polymer binder used in the composite cathode, nanoindentation measurements were conducted on composite cathodes containing different amounts of P(TFE-TTD) binder, and the results are presented in Fig. S9a and S9b. The elastic recovery ratio of the electrode without binder was 5.2 %. In contrast, the composite cathodes with 1.0, 2.0, and 3.0 wt% P(TFE-TTD) binder exhibited higher elastic recovery ratios of 7.7, 15.7, and 16.6 %, respectively. The ionic conductivities of pure Li₆PS₅Cl and Li₆PS₅Cl-based composites with varying amounts of P(TFE-TTD) binder Li₆PS₅Cl: binder = 30 - X: X by weight) were measured. As shown in Fig. S9c, the addition of polymer binder led to decreased ionic conductivities compared to that of pure Li₆PS₅Cl (1.67 mS cm⁻¹), which is attributed to the obstruction of ionic pathways in the composites. After two pre-conditioning cycles at 0.05 C, the cycling performance of composite cathodes with different P(TFE-TTD) binder contents was tested at 0.5 C and 25 °C. As shown in Fig. S9d, the cell containing 2.0 wt% P(TFE-TTD) exhibited the best cycling performance. Excessive binder (above 2.0 wt%) may hinder electron and Li⁺ ion transport within the composite cathode due to restricted conduction pathways [42]. Conversely, when the binder content is below 2.0 wt%, interfacial adhesion among the components in the electrode becomes insufficient. These results indicate that 2.0 wt% P (TFE-TTD) is the optimal content for achieving both enhanced mechanical integrity and efficient electron/ion transport within the electrode.

The cycling performance of all-solid-state cells employing 2 wt% of PTFE and P(TFE-TTD) binders was evaluated and compared. During the first pre-conditioning cycle at 0.05 C and 25 °C, the cell with P(TFE-

TTD) exhibited a higher discharge capacity of 183.8 mAh $\rm g^{-1}$ compared to 180.8 mAh $\rm g^{-1}$ for the cell using PTFE, as shown in Fig. 4a. Fig. 4b presents the voltage profiles of the P(TFE-TTD)-based cell during cycling at 0.5 C, while Fig. 4c compares the cycling performance of cells using different binders. The cell employing PTFE binder exhibited large capacity fading upon repeated cycling. By contrast, the cell with P(TFE-TTD) demonstrated 87 % capacity retention after 200 cycles, along with a stable coulombic efficiency averaging 99.5 % throughout the cycling.

The AC impedance spectra obtained before and after cycling for both cells are presented in Fig. 4d and e. In the equivalent circuit of Fig. S10, the bulk resistance of the solid electrolyte (Rb) was determined from the X-axis intercept of the spectra, and the interfacial resistances ($R_i = R_f +$ R_{ct}) were obtained from the depressed semicircle. The fitting results based on this equivalent circuit are summarized in Table S1. Before cycling, the cells with both binders exhibited similar bulk resistance, while the interfacial resistance of the PTFE-containing cell was slightly higher than that of the cell using P(TFE-TTD). Notably, a substantial difference in interfacial resistance emerged after 200 cycles. The increase in interfacial resistance for the PTFE-based cell may be attributed to the deterioration of interfacial contact among the components within the composite cathode during cycling. In contrast, the P(TFE-TTD)based cell exhibited only a slight increase in interfacial resistance, which can be ascribed to the strong binding properties of the polymer binder. These results confirm the ability of the P(TFE-TTD) binder to sustain strong interfacial adhesion among electrode components during cycling. The superior elastic and adhesive properties of the P(TFE-TTD) binder help prevent interfacial contact loss caused by mechanical stress induced by the volume changes of active materials during repeated cycling. This contributes to the maintenance of continuous electron and ion pathways within the composite cathode. These effects could be confirmed through cross-sectional SEM images of the composite cathodes before and after cycling. As shown in Fig. 5, the composite cathode incorporating the P(TFE-TTD) binder exhibited improved interfacial contact after 200 cycles compared to the electrode using PTFE, which is attributed to the strong adhesive characteristics of the P(TFE-TTD) binder.

Fig. 6a displays the discharge profiles of the all-solid-state cell with P (TFE-TTD) binder at different current rates, and the rate capabilities of cells with different binders are compared in Fig. 6b. Clearly, the cell using P(TFE-TTD) exhibited higher discharge capacities across all tested C-rates. DC-IR measurements for the cells with PTFE and P(TFE-TTD) binders were performed, as shown in Fig. 6c. The DC-IR values were determined from the slope of the voltage change versus current at various C-rates (Fig. 6d). The P(TFE-TTD)-based cell exhibited lower resistance (84.4 Ω) during both charge and discharge processes than the PTFE-based cell (103.0 Ω), indicating reduced internal resistance. This observation is consistent with the AC impedance results presented in Fig. 4d and e.

To investigate the distinct electrochemical kinetics of composite cathodes incorporating different binders, DC polarization measurements were conducted using symmetric cell configurations. By employing both electron-blocking and ion-blocking cell setups, we were able to decouple the contributions of ionic and electronic conductivity within the cathode materials [43]. Electronic conductivity was determined using DC polarization with an ion-blocking cell configuration. As shown in Fig. S11a and S11b, the current exhibited a step-function increase in response to a constant applied voltage and reversed instantaneously upon voltage switching. This behavior is indicative of dominant electronic conduction. As illustrated in Fig. S11c, the composite cathode employing P (TFE-TTD) exhibited higher electronic conductivity compared to the PTFE-based electrode. The improved electronic transport is attributed to the uniform dispersion of P(TFE-TTD) and conductive carbon. Subsequently, ionic conductivity was evaluated using an electron-blocking cell. As shown in Fig. S12a and S12b, the voltage profiles of cells containing PTFE and P(TFE-TTD) binders demonstrated time-dependent behavior, consistent with ionic transport processes. Using Ohm's law,

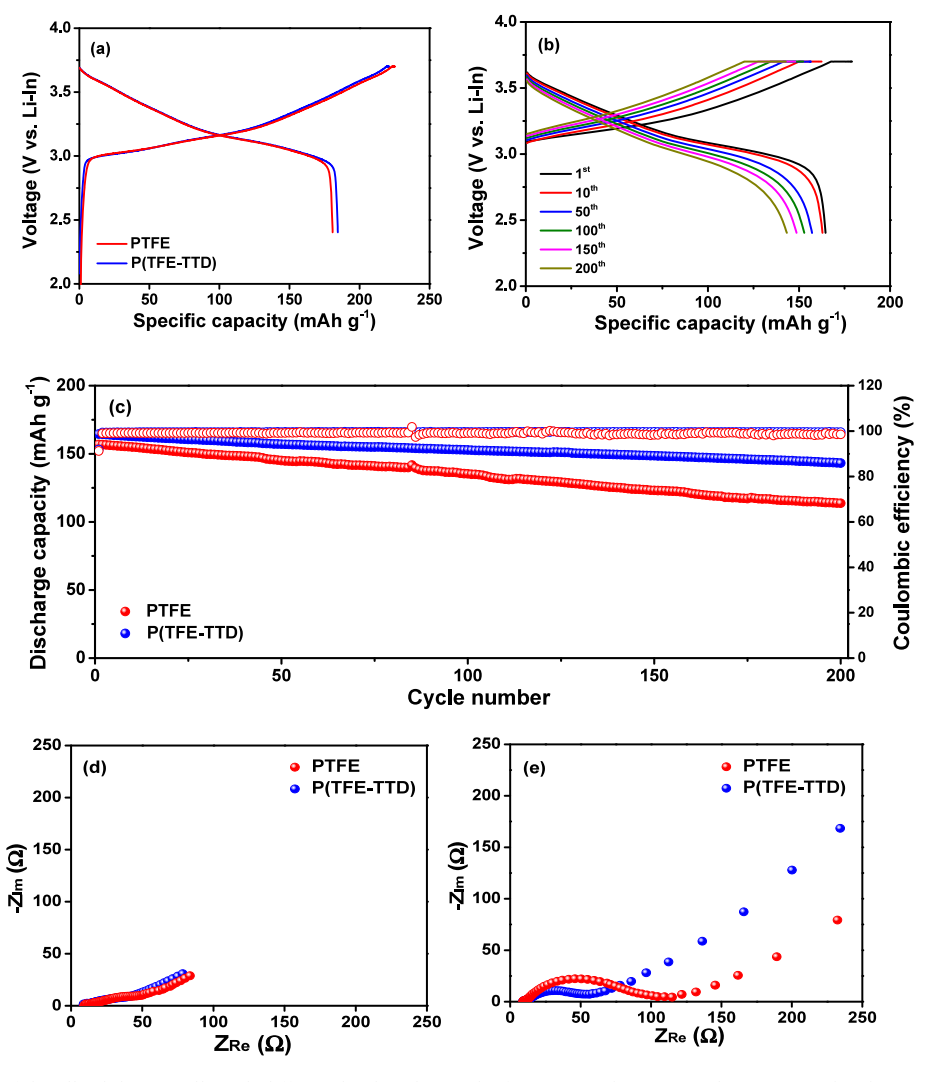


Fig. 4. (a) Voltage profiles of the all-solid-state cells with different binders during the first pre-conditioning cycle at 0.05 C. (b) Charge and discharge curves of the cell with P(TFE-TTD) at 0.5 C. (c) Cycling performance of the cells with different binders at 0.5 C. AC impedance spectra of the cells with different binders (d) before and (e) after 200 cycles.

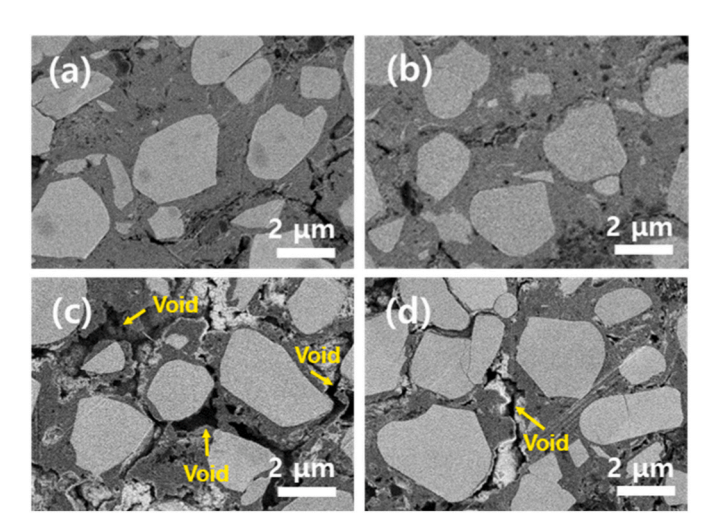


Fig. 5. Cross-sectional SEM images of composite cathodes prepared with (a) PTFE and (b) P(TFE-TTD) binders before cycling. Cross-sectional SEM images of composite cathodes prepared with (c) PTFE and (d) P(TFE-TTD) binders after 200 cycles.

ionic resistance was calculated from the i-V plots and subsequently translated into ionic conductivity. As presented in Fig. S12c, the P (TFE-TTD) composite cathode exhibited superior ionic conductivity compared to the PTFE-containing cathode, further supporting the superior ion transport characteristics of the P(TFE-TTD)-based composite cathode. In addition, we measured the ionic conductivities of pure $\text{Li}_6\text{PS}_5\text{Cl}$, $\text{Li}_6\text{PS}_5\text{Cl}$ with PTFE, and $\text{Li}_6\text{PS}_5\text{Cl}$ with P(TFE-TTD) composites (Li $_6\text{PS}_5\text{Cl}$: binder = 25 : 2 by weight) using electrochemical impedance spectroscopy. The results are presented in Fig. S13. The composite consisting of Li $_6\text{PS}_5\text{Cl}$ and P(TFE-TTD) exhibited higher ionic conductivity than the one combined with PTFE. This improvement can be attributed to the preservation of ion-conduction pathways in Li $_6\text{PS}_5\text{Cl}$, resulting from better interfacial contact enabled by the superior adhesive properties of P(TFE-TTD).

The superior cycling performance of the all-solid-state cell with an NCM composite cathode using the P(TFE-TTD) binder, as demonstrated by the preceding results, is schematically represented in Fig. 7. PTFE, a relatively weak adhesive, tends to distribute non-uniformly within the composite cathode and acts as an electronically and ionically insulating material, thereby impeding efficient conduction pathways. In contrast, P (TFE-TTD) is uniformly dispersed throughout the composite cathode, promoting improved interfacial contacts between cathode components due to its strong interaction with active materials and conductive

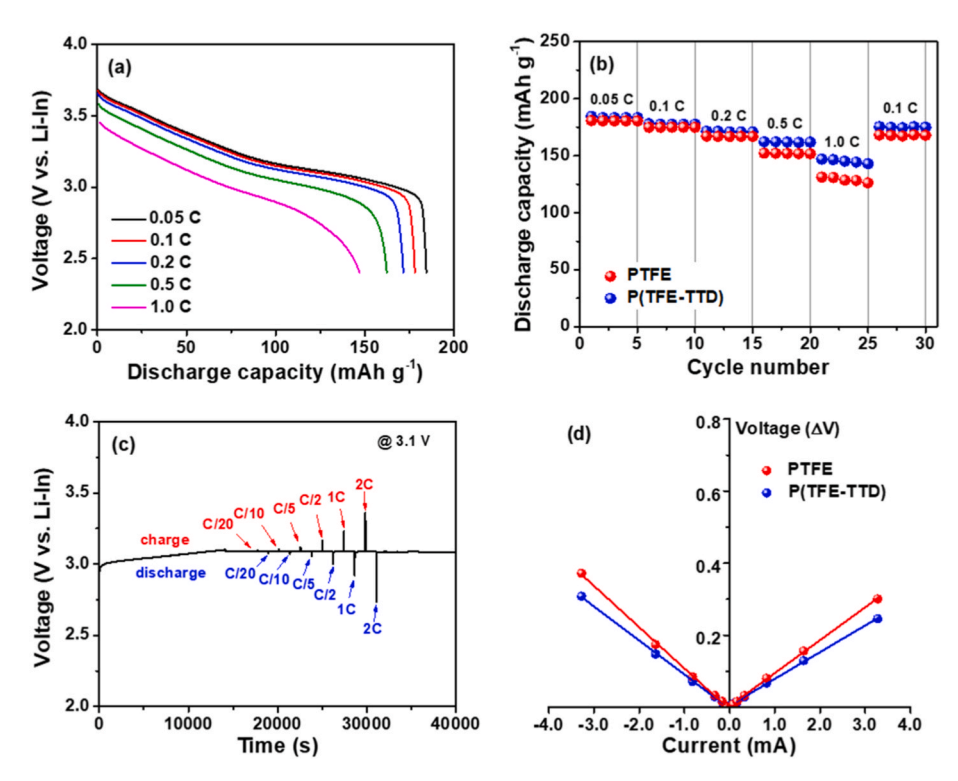


Fig. 6. (a) Discharge curves of the all-solid-state cells prepared with P(TFE-TTD). (b) Rate capabilities of the cells with different binders at 25 °C. (c) Voltage responses of the cells prepared with P(TFE-TTD) during DC-IR experiment at 25 °C. (d) Plots of the voltage change vs current of cells prepared with different binders.

(a) PTFE binder – Line contact

NCM LPSCI Carbon nanofiber PTFE P(TFE-TTD)

Fig. 7. Schematic presentation of the composite cathodes employing (a) PTFE and (b) P(TFE-TFE) binders.

additives. This enhanced interfacial adhesion, combined with the facilitation of ${\rm Li}^+$ transport, results in improved electrochemical performance. The increased electronic and ionic conductivities, along with the reduced interfacial resistance associated with the P(TFE-TTD) binder, collectively contribute to lower internal resistance during cycling, ultimately leading to enhanced performance and cycling stability of the all-solid-state battery.

4. Conclusions

Composite cathodes were prepared using a dry process with the adhesive P(TFE-TTD) binder. Its excellent adhesive properties and uniform distribution in the composite cathode ensured strong interfacial contacts among the solid electrolyte, active material, and conducting carbon. Comprehensive mechanical and morphological analyses revealed that P(TFE-TTD) effectively accommodates the mechanical stress associated with the volume changes of active materials during cycling. This mechanical robustness helps maintain interfacial integrity and electrical conductivity during extended cycling. Consequently, allsolid-state batteries assembled with NCM composite cathodes incorporating P(TFE-TTD) exhibited significantly improved electrochemical performance, including higher capacity retention, enhanced cycling stability, and superior rate capability compared to their PTFE-based counterparts. These findings highlight P(TFE-TTD) as a promising binder for the dry fabrication of high-performance composite cathodes in next-generation ASSLBs.

CRediT authorship contribution statement

Jiho Cha: Writing – original draft, Investigation, Data curation, Conceptualization. **Young-Jun Lee:** Validation, Methodology, Investigation, Data curation. **Dong-Won Kim:** Writing – review & editing, Project administration, Investigation, Funding acquisition, Conceptualization.

Declaration of competing interest

The authors declare that they have no known competing financial interests or personal relationships that could have appeared to influence the work reported in this paper.

Acknowledgments

This work was supported by the National Research Foundation of Korea (RS-2024-00454354) and Technology Innovation Program (20023145) funded by the Ministry of Trade, Industry, and Energy (MOTIE, Korea).

Appendix A. Supplementary data

Supplementary data to this article can be found online at https://doi.org/10.1016/j.mtener.2025.102009.

Data availability

Data will be made available on request.

References

- O. Ellabban, H. Abu-Rub, F. Blaabjerg, Renewable energy resources: current status, future prospects and their enabling technology, Renew. Sustain. Energy Rev. 39 (2014) 748–764. https://doi.org/10.1016/j.rser.2014.07.113.
- [2] M. Gutsch, J. Leker, Global warming potential of lithium-ion battery energy storage systems: a review, J. Energy Storage 52 (2022) 105030, https://doi.org/10.1016/j. est.2022.105030.
- [3] T. Kim, W. Song, D.-Y. Son, L.K. Ono, Y. Qi, Lithium-ion batteries: outlook on present, future, and hybridized technologies, J. Mater. Chem. A 7 (2019) 2942–2964, https://doi.org/10.1039/C8TA10513H.
- [4] B. Diouf, R. Pode, Potential of lithium-ion batteries in renewable energy, Renew. Energy 76 (2015) 375–380, https://doi.org/10.1016/j.renene.2014.11.058.
- [5] J. Wen, D. Zhao, C. Zhang, An overview of electricity powered vehicles: Lithiumion battery energy storage density and energy conversion efficiency, Renew. Energy 162 (2020) 1629–1648, https://doi.org/10.1016/j.renene.2020.09.055.
- [6] M. Killer, M. Farrokhseresht, N.G. Paterakis, Implementation of large-scale Li-ion battery energy storage systems within the EMEA region, Appl. Energy 260 (2020) 114166. https://doi.org/10.1016/j.apenergy.2019.114166.
- [7] Y. Chen, Y. Kang, Y. Zhao, L. Wang, J. Liu, Y. Li, Z. Liang, X. He, X. Li, N. Tavajohi, B. Li, A review of lithium-ion battery safety concerns: the issues, strategies, and testing standards, J. Energy Chem. 59 (2021) 83–99, https://doi.org/10.1016/j. iechem.2020.10.017.
- [8] C. Arbizzani, G. Gabrielli, M. Mastragostino, Thermal stability and flammability of electrolytes for lithium-ion batteries, J. Power Sources 196 (2011) 4801–4805, https://doi.org/10.1016/j.jpowsour.2011.01.068.
- [9] Z. Gao, H. Sun, L. Fu, F. Ye, Y. Zhang, W. Luo, Y. Huang, Promises, challenges, and recent progress of inorganic solid-state electrolytes for all-solid-state lithium batteries, Adv. Mater. 30 (2018) 1705702, https://doi.org/10.1002/ adms.201705703
- [10] Y. Chen, K. Wen, T. Chen, X. Zhang, M. Armand, S. Chen, Recent progress in all-solid-state lithium batteries: the emerging strategies for advanced electrolytes and their interfaces, Energy Storage Mater. 31 (2020) 401–433, https://doi.org/10.1016/j.ensm.2020.05.019.
- [11] Z. Guo, H. Zhao, Y. Xiao, S. Liang, X. Zhang, N. Wang, J. Yang, X. Huang, Recent progress of thin solid-state electrolytes and applications for solid-state lithium pouch cells, mater, Today Energy 48 (2025) 101801, https://doi.org/10.1016/j. mtener.2025.101801.
- [12] L. Tian, J.-W. Kim, D.-W. Kim, Solid hybrid electrolytes based on conductive oxides and polymer electrolytes for all-solid-lithium batteries, Mater. Chem. Front. 8 (2024) 455–484, https://doi.org/10.1039/d3qm00736g.
- [13] X. Yao, D. Liu, C. Wang, P. Long, G. Peng, Y.-S. Hu, H. Li, L. Chen, X. Xu, High-energy all-solid-state lithium batteries with ultralong cycle life, Nano Lett. 16 (2016) 7148–7154, https://doi.org/10.1021/acs.nanolett.6b03448.
- [14] D. Li, H. Liu, Y. Liang, C. Wang, L.-Z. Fan, Challenges and developments of high energy density anode materials in sulfide-based solid-state batteries, Chemelectrochem 9 (2022) e202200923, https://doi.org/10.1002/ psla.20200023
- [15] C. Wang, J. Liang, Y. Zhao, M. Zheng, X. Li, X. Sun, All-solid-state lithium batteries enabled by sulfide electrolytes: from fundamental research to practical engineering design, Energy Environ. Sci. 14 (2021) 2577–2619, https://doi.org/10.1039/ D1FE00551K
- [16] H.-T. Sim, M.-K. Oh, H.-J. Kim, Y.-E. Park, Y.-S. Cho, J. Choi, S.-J. Park, D.-W. Kim, Surface-modified lithium enabling high-performance all-solid-state lithium metal batteries, ACS Energy Lett. 10 (2025) 2277–2284, https://doi.org/10.1021/ acsenergylett.5c00656.

- [17] C. Wang, X. Zhao, D. Li, C. Yan, Q. Zhang, L.-Z. Fan, Anion-modulated ion conductor with chain conformational transformation for stabilizing interfacial phase of high-voltage lithium metal batteries, Angew. Chem. Int. Ed. 63 (2024) e202317856, https://doi.org/10.1002/anie.202317856.
- [18] B. Tao, C. Ren, H. Li, B. Liu, X. Jia, X. Dong, S. Zhang, H. Chang, Thio-/LISICON and LGPS-type solid electrolytes for all-solid-state lithium-ion batteries, Adv. Funct. Mater. 32 (2022) 2203551, https://doi.org/10.1002/adfm.202203551.
- [19] Y.-J. Lee, S.-B. Hong, H.-J. Lee, H.-T. Sim, Y. Kim, S. Kim, D.-W. Kim, Flexible and thin sulfide-based solid electrolyte sheet with Li⁺-ion conductive polymer network for all-solid-state lithium-ion batteries, Chem. Eng. J. 477 (2023) 146983, https://doi.org/10.1016/j.cei.2023.146983.
- [20] A. Sakuda, A. Hayashi, M. Tatsumisago, Sulfide solid electrolyte with favorable mechanical property for all-solid-state lithium battery, Sci. Rep. 3 (2013) 2261, https://doi.org/10.1038/srep02261.
- [21] C. Yu, F. Zhao, J. Luo, L. Zhang, X. Sun, Recent development of lithium argyrodite solid-state electrolytes for solid-state batteries: synthesis, structure, stability and dynamics, Nano Energy 83 (2021) 105858, https://doi.org/10.1016/j. nanoen.2021.105858.
- [22] J. Lau, R.H. DeBlock, D.M. Butts, D.S. Ashby, C.S. Choi, B.S. Dunn, Sulfide solid electrolytes for lithium battery applications, Adv. Energy Mater. 8 (2018) 1800933, https://doi.org/10.1002/aenm.201800933.
- [23] S.-B. Hong, Y.-R. Jang, Y.-C. Jung, W. Cho, D.-W. Kim, Sulfide-based flexible solid electrolyte enhancing cycling performance of all-solid-state lithium batteries, ACS Appl. Energy Mater. 7 (2024) 5193–5201, https://doi.org/10.1021/ acsaem.4c00547.
- [24] X. Wang, L. Ye, C.-W. Nan, X. Li, Effect of solvents on a Li₁₀GeP₂S₁₂-Based composite electrolyte via solution method for solid-state battery applications, ACS Appl. Mater. Interfaces 14 (2022) 46627–46634, https://doi.org/10.1021/acsami.2c1.920
- [25] S.-B. Hong, Y.-R. Jang, H. Kim, Y.-C. Jung, G. Shin, H.J. Hah, W. Cho, Y.-K. Sun, D.-W. Kim, Wet-processable binder in composite cathode for high energy density all-solid-state lithium batteries, Adv. Energy Mater. 14 (2024) 2400802, https://doi.org/10.1002/aenm.202400802.
- [26] G. Sahu, Z. Lin, J. Li, Z. Liu, N. Dudney, C. Liang, Air-stable, high-conduction solid electrolytes of arsenic-substituted Li₄SnS₄, Energy Environ. Sci. 7 (2014) 1053–1058, https://doi.org/10.1039/C3EE43357A.
- [27] Y.-T. Chen, M.A.T. Marple, D.H.S. Tan, S.-Y. Ham, B. Sayahpour, W.-K. Li, H. Yang, J.B. Lee, H.J. Hah, E.A. Wu, J.-M. Doux, J. Jang, P. Ridley, A. Cronk, G. Deysher, Z. Chen, Y.S. Meng, Investigating dry room compatibility of sulfide solid-state electrolytes for scalable manufacturing, J. Mater. Chem. A 10 (2022) 7155–7164, https://doi.org/10.1039/D1TA09846B.
- [28] Y. Lu, C.-Z. Zhao, H. Yuan, J.-K. Hu, J.-Q. Huang, Q. Zhang, Dry electrode technology, the rising star in solid-state battery industrialization, Matter 5 (2022) 876–898, https://doi.org/10.1016/j.matt.2022.01.011.
- [29] Y. Li, Y. Wu, Z. Wang, J. Xu, T. Ma, L. Chen, H. Li, F. Wu, Progress in solvent-free dry-film technology for batteries and supercapacitors, Mater. Today 55 (2022) 92–109. https://doi.org/10.1016/j.mattod.2022.04.008.
- [30] C. Wang, R. Yu, H. Duan, Q. Lu, Q. Li, K.R. Adair, D. Bao, Y. Liu, R. Yang, J. Wang, S. Zhao, H. Huang, X. Sun, Solvent-free approach for interweaving freestanding and ultrathin inorganic solid electrolyte membranes, ACS Energy Lett. 7 (2022) 410–416, https://doi.org/10.1021/acsenergylett.1c02261.
- [31] Y. Li, Y. Wu, Z. Wang, J. Xu, T. Ma, L. Chen, H. Li, F. Wu, Progress in solvent-free dry-film technology for batteries and supercapacitors, Mater. Today 55 (2022) 92–109, https://doi.org/10.1016/j.mattod.2022.04.008.
- [32] Y.-J. Lee, S.-Y. Kim, W.-J. Song, J. Cha, D.-W. Kim, Enhancing the cycling performance of sulfide-based all-solid-state lithium batteries via molecular weightdependent fibrillation of PTFE binders, Mater. Today Energy 51 (2025) 101914, https://doi.org/10.1016/j.mtener.2025.101914.
- [33] S. Thieme, J. Bruckner, I. Bauer, M. Oschatz, L. Borchardt, H. Althues, S. Kaskel, High capacity micro-mesoporous carbon–sulfur nanocomposite cathodes with enhanced cycling stability prepared by a solvent-free procedure, J. Mater. Chem. A. 1 (2013) 9225–9234. https://doi.org/10.1039/C3TA10641A.
- [34] S.-B. Hong, Y.-J. Lee, U.-H. Kim, C. Bak, Y.M. Lee, W. Cho, H.J. Hah, Y.-K. Sun, D.-W. Kim, All-solid-state lithium batteries: Li⁺-conducting ionomer binder for dry-processed composite cathodes, ACS Energy Lett. 7 (2022) 1092–1100, https://doi.org/10.1021/acsenergylett.1c02756.
- [35] L. Hu, Y. Ren, C. Wang, J. Li, Z. Wang, F. Sun, J. Ju, J. Ma, P. Han, S. Dong, G. Cui, Fusion bonding technique for solvent-free fabrication of all-solid-state battery with ultrathin sulfide electrolyte, Adv. Mater. 36 (2024) 2401909, https://doi.org/ 10.1002/adma.202401909
- [36] S.-B. Hong, Y.-J. Lee, H.-J. Lee, H.-T. Sim, H. Lee, Y.M. Lee, D.-W. Kim, Exploring the cathode active materials for sulfide-based all-solid-state lithium batteries with high energy density, Small 20 (2024) 2304747, https://doi.org/10.1002/ smll 202304747
- [37] J. Cha, S. Kim, U.T. Nakate, D.-W. Kim, Highly conductive composite cathode prepared by dry process using Nafion-Li ionomer for sulfide-based all-solid-state lithium batteries, J. Power Sources 613 (2024) 234914, https://doi.org/10.1016/j. jpowsour.2024.234914.
- [38] J. Piwowarczyk, R. Jedrzejewski, D. Moszynski, K. Kwiatkowski, A. Niemczyk, J. Baranowska, XPS and FTIR studies of polytetrafluoroethylene thin films obtained by physical methods, Polymers 11 (2019) 1629, https://doi.org/10.3390/ polym11101629.
- [39] S.A. Perusich, Fourier transform infrared spectroscopy of perfluorocarboxylate polymers, Macromolecules 33 (2000) 3431–3440, https://doi.org/10.1021/ ma990424h.

- [40] Y. Zhang, F. Huld, S. Lu, C. Jektvik, F. Lou, Z. Yu, Revisiting polytetrafluorethylene binder for solvent-free lithium-ion battery anode fabrication, Batteries 8 (2022) 57, https://doi.org/10.3390/batteries8060057
- https://doi.org/10.3390/batteries8060057.

 [41] X. Wang, S. Chen, K. Zhang, L. Huang, H. Shen, Z. Chen, C. Rong, G. Wang, Z. Jiang, A polytetrafluoroethylene-based solvent-free procedure for the manufacturing of lithium-ion batteries, Materials 16 (2023) 7232, https://doi.org/10.3300/ma16227332
- [42] J. Zhang, H. Zhong, C. Zheng, Y. Xia, C. Liang, H. Huang, Y. Gan, X. Tao, W. Zhang, All-solid-state batteries with slurry coated LiNi_{0.8}Co_{0.1}Mn_{0.1}O₂ composite cathode and Li₀PS₅Cl electrolyte: effect of binder content, J. Power Source 391 (2018) 73–79. https://doi.org/10.1016/i.jnowsour.2018.04.069.
- 73–79, https://doi.org/10.1016/j.jpowsour.2018.04.069.
 [43] L. Zhang, Y. Dai, C. Li, Y. Dang, R. Zheng, Z. Wang, Y. Wang, Y. Cui, H. Arandiyan, Z. Shao, H. Sun, Q. Zhuang, Y. Liu, Recent advances in electrochemical impedance spectroscopy for solid-state batteries, Energy Storage Mater. 69 (2024) 103378, https://doi.org/10.1016/j.ensm.2024.103378.